AIAA JOURNAL
Vol. 44, No. 6, June 2006

Adaptive Control of Nonlinear Free Vibrations of Composite Plates Using Piezoelectric Actuators

Qinqin Li,* Thongchai Phairoh,† Jen-Kuang Huang,‡ and Chuh Mei§
Old Dominion University, Norfolk, Virginia 23529

A coupled structural–electrical finite element modal formulation is employed for the control of nonlinear free vibrations of beams and composite plates. Multiple modes of the nonlinear free vibration are considered in closed-loop simulations. Two different controllers are designed and investigated for the suppression of nonlinear free vibrations. The first is the position output feedback controller comprising a linear quadratic regulator (LQR) and an extended Kalman filter (EKF). The EKF is used to consider the nonlinear state-space matrix and has a gain sequence evaluated online. The second controller is the output feedback adaptive LQR/EKF controller. This adaptive controller includes an adaptive modal frequency identification and state estimation algorithm. Numerical simulations show that the adaptive LQR/EKF controller with system identification is effective in suppressing nonlinear free vibrations of a beam and a composite plate with unpredictable sudden frequency changes. The placement of piezoelectric self-sensing actuators is based on three approaches: one is the norm of optimal feedback control gain matrix method, the second is the H_2 norm, and the last one is the norm of Kalman filter estimation gain method.

Nomenclature

$[A]$, $[B]$, $[D]$	=	in-plane, coupling, and bending laminated stiffness matrices
D_{ik}	=	electric displacement
$\{d\}$	=	piezoelectric charge constant vector
E, E_1, E_2, E_p	=	Young's moduli
E_{ik}	=	electric field
G, G_{12}, G_p	=	shear moduli
h	=	beam or composite plate thickness
$[K_w]$	=	combined system linear stiffness matrix
$[K1]$, $[K2]$	=	combined system first- and second-order nonlinear stiffness matrices
$[\bar{K}]$	=	modal linear stiffness matrix
$[\bar{K}_{qq}]$	=	modal nonlinear stiffness matrix
$[k]$, $[K]$	=	element and system stiffness matrices
$[k1]$, $[k2]$	=	element first- and second-order nonlinear stiffness matrices
$[\bar{M}]$	=	modal mass matrix
$[m]$, $[M]$	=	element and system mass matrices
$\{N\}$, $\{M\}$	=	force and moment resultant vectors
$\{p_\varphi\}$, $\{P_\varphi\}$	=	element and system electric force vectors
$[\bar{Q}]$	=	transformed lamina reduced stiffness matrix
$\{q\}$	=	natural modal coordinate vector
u, v	=	in-plane displacements
$\{w\}$, $\{W\}$	=	element and system nodal displacements
ϵ	=	dielectric permittivity
$\{\varepsilon\}$	=	strain vector
$\{\kappa\}$	=	bending curvature vector
ν, ν_1, ν_2	=	Poisson's ratios
ρ, ρ_p	=	mass densities
$\{\sigma\}$	=	stress vector
$\{\bar{\phi}\}$	=	modal electric force vector
ω	=	frequency

Presented as Paper 2005-2120 at the AIAA/ASME/ASCE/AHS/ASC 46th Dynamics and Materials Conference, Austin, TX, 18–21 April 2005; received 24 August 2005; revision received 29 November 2005; accepted for publication 29 November 2005.

*Research Assistant, Department of Aerospace Engineering.
†Research Assistant, Department of Mechanical Engineering.
‡Professor, Department of Mechanical Engineering. Member AIAA.
§Professor, Department of Aerospace Engineering. Associate Fellow AIAA.

I. Introduction

ACTIVE control of vibration of flexible structures has important applications in engineering, especially in the aerospace and automotive fields. Most investigations use linear control methods for linear models. However, nonlinearity has to be considered due to large elastic motions that influence the structural response tremendously but that have been very seldom considered in vibration controls. The first description of large-amplitude vibration of beams can be traced in the literature to Woinowsky-Krieger,[1] who considered the free vibration of a simply supported beam with the effect of axial force and solved the nonlinear equation of motion by using a single-mode approach and elliptic function. He then gave the relationship between vibration amplitude and the ratio of nonlinear frequency to natural frequency. Other investigators used the perturbation method,[2] the Ritz–Galerkin technique (see Ref. 3), assumed space mode and assumed time mode,[4] etc., to solve analytically the nonlinear free vibrations of beams for different boundary conditions. Mei[5] presented a finite element analysis for nonlinear vibrations of beams and obtained remarkable agreement with the experimental data. In 1994, Srirangarajan[6] presented two methods, the multiple scales and the ultraspherical polynomial approximation procedures, to solve nonlinear free vibrations of simply supported uniform beams; results were compared with nine other previous methods. Shi et al.[7] presented a finite element modal method that is able to obtain the Duffing-type modal equations more easily than the classic continuum partial differential equation Galerkin's method. They concluded that, for simply supported beams, a single-mode solution with elliptic function method is accurate; for other beam and plate structures, multiple modes are needed.

Saha et al.[8] recently employed the von Kármán nonlinear strain–displacement relations and obtained large-amplitude free vibration of square plates for different boundary conditions. They solved the corresponding static problem through an iterative scheme using a relaxation parameter and then solved the dynamic problem as a standard eigenvalue problem. There are many approximation methods[9] presented for this topic. Mei[10] applied the finite element method. Chia[11] presented an excellent review in 1988 for the geometrically

nonlinear behavior of composite plates. Shi et al.[7] presented a time-domain multiple modal formulation based on the finite element method for large-amplitude free vibrations of thin composite plates. Recently, Alhazza and Alhazza[12] presented a review of the recent progress in vibrations of plates and shells. Harada et al.[13] used the finite element method to derive a set of reduced-order nonlinear modal equations of plates, and they obtained the dominant nonlinear in-plane pseudomodes by an approximate approach using the Newton–Raphson method.

For active control of vibrations, vibration controllers can usually be designed in terms of modal modes or wave motion due to the two descriptions of vibrations. Generally, modal control aims to control the global behavior of the structures whereas wave control aims to control the flow of vibration energy through the structures.[14] There are many publications in the literature on wave control.[14,15] However, when wave control efficiently suppresses vibrations on one part of the structures, global responses of the control may introduce vibrations on other parts because wave control does not consider the global motions of the structures. To avoid this drawback of wave control, modal control becomes another attractive method. Although modal control may have the main disadvantage of spillover with the implementation of smart structures, the spillover is manageable. Currently, modal control is realized by many methods: pole placement,[16] optimal control,[17] robust control,[18] adaptive control,[19] and intelligent control.[20] Most of these methods have good simulation or testing results in the linear model, or in a single-mode nonlinear model.

To realize active control, sensors and actuators are the necessary parts of the whole control system. Recently, smart structures have been broadly used. Among all of the smart structures, piezoelectric materials are most commonly used in the field. At first, monolithic piezoelectric elements such as PZT, PLZT, and PVDF were used to control vibrations of beams[21] and plates.[22] Recently, piezoelectric fiber composite materials such as 1–3 composites, active fiber composites, and macrofiber composites (MFC) have been explored.[23] With the piezoelectric fiber composite nature and interdigitated electrodes, they could increase actuation authority, flexibility, and the ability to impose twisting deformation onto structures. Many applications of these piezocomposite materials have been presented.[24] In fact, piezoelectric materials cannot only be used as actuators or sensors in active control of vibrations, but they can also combine both functions on one device, namely, the self-sensing actuator, which is perfectly collocated and can be effectively modeled and implemented in vibration suppression.[25] To suppress vibrations efficiently, the locations of actuators and sensors are also very important. Many methods for the optimal placement of actuators and sensors have been developed; for example, the controllability method includes the modal controllability,[26] modal and system controllability,[27] spatial controllability,[28] and H_∞ analytical bound approaches.[29] Another class of methods is the performance index method.[30] Other special algorithms, such as the genetic algorithm[31] and simulated annealing optimization algorithm, are also used.[32] Most of the methods are, however, efficient for linear models. In this paper, the optimal placement of the self-sensing actuators, the norm of optimal feedback control gain matrix (NFCG) method,[33,34] and the H_2 norm method are employed.[28]

In the present research, multiple-mode nonlinear free vibrations of an isotropic beam and a composite plate of clamped boundary conditions are modeled with the finite element method. The linear quadratic regulator (LQR) plus an extended Kalman filter (EKF) with system identification is implemented for control. Because the objects are nonlinear systems, a linear estimator cannot consider the nonlinear effects, and it will deteriorate the state estimation performance. Thus, we choose the nonlinear estimator EKF to give the estimation. Numerical results have demonstrated the excellent performance of the EKF. Because the initial state estimation is vital for the EKF to estimate the states for the whole control system, accurate initially estimated states are necessary for the nonlinear estimation. These can be obtained from an adaptive system identification algorithm.

II. System Modeling

A. Strain–Displacement Relations

A clamped isotropic beam and a clamped composite plate are modeled by using the Bogner–Fox–Schmit[35] (BFS) C^1 conforming rectangular elements. There are 16 bending degrees of freedom (DOF) $\{w_b\}_{16\times 1}$, and 8 in-plane DOF $\{w_m\}_{8\times 1}$ in each BFS element

$$\{w_b\} = \left\{w_1 w_2 w_3 w_4 w_{x_1} w_{x_2} w_{x_3} w_{x_4} w_{y_1} w_{y_2} w_{y_3} w_{y_4} w_{xy_2} w_{xy_3} w_{xy_3} w_{xy_4}\right\}^T$$

$$\{w_m\} = \{u_1 u_2 u_3 u_4 v_1 v_2 v_3 v_4\}^T \tag{1}$$

The von Kármán large-deflection theory is used to account for nonlinear vibration of beams and plates. The strains can be represented as

$$\{\varepsilon\} = \begin{Bmatrix} \varepsilon_x \\ \varepsilon_y \\ \gamma_{xy} \end{Bmatrix} = \begin{Bmatrix} \varepsilon_x^0 \\ \varepsilon_y^0 \\ \gamma_{xy}^0 \end{Bmatrix} + z \begin{Bmatrix} \kappa_x \\ \kappa_y \\ \kappa_{xy} \end{Bmatrix} = \{\varepsilon^0\} + z\{\kappa\} \tag{2}$$

The strain vector can be written in terms of the displacement functions as

$$\{\varepsilon\} = \begin{Bmatrix} u_{,x} \\ v_{,y} \\ u_{,y} + v_{,x} \end{Bmatrix} + \frac{1}{2} \begin{Bmatrix} w_{,x}^2 \\ w_{,y}^2 \\ 2w_{,x} w_{,y} \end{Bmatrix} + z \begin{Bmatrix} -w_{,xx} \\ -w_{,yy} \\ -2w_{,xy} \end{Bmatrix} \tag{3}$$

B. Constitutive Equations

For a general kth piezoelectric layer embedded in a laminated composite plate, we can write the stress–strain relationships derived from the classical laminate plate theory.[36] Because the composite plates are thin, that is, the ratio of length or width over thickness of the plate is greater than 50, the shear deformation can be neglected. Also, the isotropic beam is the special case of the composite plate. Detailed derivation of these equations can also be found in Bevan,[37] Abdel-Motagaly,[25] and Guo[38]:

$$\{\sigma\}_k = \begin{Bmatrix} \sigma_x \\ \sigma_y \\ \tau_{xy} \end{Bmatrix}_k = \begin{bmatrix} \bar{Q}_{11} & \bar{Q}_{12} & \bar{Q}_{16} \\ \bar{Q}_{12} & \bar{Q}_{22} & \bar{Q}_{26} \\ \bar{Q}_{16} & \bar{Q}_{26} & \bar{Q}_{66} \end{bmatrix}_k \left\{ \begin{Bmatrix} \varepsilon_x \\ \varepsilon_y \\ \gamma_{xy} \end{Bmatrix} - E_{ik} \begin{Bmatrix} d_x \\ d_y \\ d_{xyk} \end{Bmatrix} \right\} \tag{4}$$

where $[\bar{Q}_{ij}]_k$ is the transformed reduced lamina stiffness matrix comprising the material properties and the influence of the lamination angle. E is the electric field and $\{d\}$ is the transformed piezoelectric charge constant. For a general composite layer, simply set $E_{3k} = 0$ in Eq. (4).

The electrical displacement for the kth piezoelectric layer can be written as

$$D_{ik} = [d_x \quad d_y \quad d_{xy}]_k \begin{bmatrix} \bar{Q}_{11} & \bar{Q}_{12} & \bar{Q}_{16} \\ \bar{Q}_{12} & \bar{Q}_{22} & \bar{Q}_{26} \\ \bar{Q}_{16} & \bar{Q}_{26} & \bar{Q}_{66} \end{bmatrix}_k \begin{Bmatrix} \varepsilon_x \\ \varepsilon_y \\ \gamma_{xy} \end{Bmatrix} + \left(\varepsilon_{ii}^{\varepsilon}\right)_k E_{ik} \tag{5}$$

where the subscript $i = 3$ for traditional PZT and $i = 1$ for MFC actuators for both Eqs. (4) and (5). D and ϵ are the electric flux density and dielectric permittivity, respectively.

The electric field E can be related to generalized electrical DOF $\{w_\varphi\}_{np\times 1}$ as

$$\begin{Bmatrix} E_{i1} \\ \vdots \\ E_{ik} \\ \vdots \\ E_{inp} \end{Bmatrix} = - \begin{bmatrix} \frac{1}{h_1} & \cdots & 0 \\ \vdots & \cdots & \vdots \\ \vdots & \frac{1}{h_k} & \vdots \\ \vdots & \cdots & \vdots \\ 0 & \cdots & \frac{1}{h_{np}} \end{bmatrix} \begin{Bmatrix} V_1 \\ \vdots \\ V_k \\ \vdots \\ V_{np} \end{Bmatrix}$$

$$= - \begin{bmatrix} \frac{1}{h_1} & \cdots & 0 \\ \vdots & \cdots & \vdots \\ \vdots & \frac{1}{h_k} & \vdots \\ \vdots & \cdots & \vdots \\ 0 & \cdots & \frac{1}{h_{np}} \end{bmatrix} \{w_\phi\} \tag{6}$$

where h_k expresses the thickness of the kth piezoelectric layer for traditional PZT but means electrode spacing of the interdigital electrodes for MFC. Note that np is the total number of piezoelectric layers.

C. Resultant Forces and Moments

The stress resultants per unit length are defined as

$$(\{N\},\{M\}) = \int_{-h/2}^{h/2} \{\sigma\}_k (1, z)\, \mathrm{d}z \tag{7}$$

After substituting Eq. (4) into the preceding equation, we have

$$\begin{Bmatrix} N \\ M \end{Bmatrix} = \begin{bmatrix} [A] & [B] \\ [B] & [D] \end{bmatrix} \begin{Bmatrix} \varepsilon^0 \\ \kappa \end{Bmatrix} - \begin{Bmatrix} N_\phi \\ M_\phi \end{Bmatrix} \tag{8}$$

where $[A]$, $[B]$, and $[D]$ are the laminate extension, coupled extension–bending, and bending matrices. $\{N_\phi\}$ and $\{M_\phi\}$ are the piezoceramic force and moment vectors.

D. Element Equations

The element equations of motion[37] are derived by the principle of virtual work

$$\begin{bmatrix} [m_b] & 0 & 0 \\ 0 & [m_m] & 0 \\ 0 & 0 & 0 \end{bmatrix} \begin{Bmatrix} \ddot{w}_b \\ \ddot{w}_m \\ \ddot{w}_\varphi \end{Bmatrix} + \left(\begin{bmatrix} [k_b] & [k_{bm}] & [k_{b\phi}] \\ [k_{mb}] & [k_m] & [k_{m\phi}] \\ [k_{\phi b}] & [k_{\phi m}] & [k_\phi] \end{bmatrix} \right.$$

$$- \begin{bmatrix} [k1_{N\phi}] & 0 & 0 \\ 0 & 0 & 0 \\ 0 & 0 & 0 \end{bmatrix} + \begin{bmatrix} [k1_{NB}] + [k1_{Nm}] & [k1_{bm}] & [k1_{b\phi}] \\ [k1_{mb}] & 0 & 0 \\ [k1_{\phi b}] & 0 & 0 \end{bmatrix}$$

$$\left. - \begin{bmatrix} [k2_b] & 0 & 0 \\ 0 & 0 & 0 \\ 0 & 0 & 0 \end{bmatrix} \right) \begin{Bmatrix} w_b \\ w_m \\ w_\phi \end{Bmatrix} = \begin{Bmatrix} 0 \\ 0 \\ p_\phi \end{Bmatrix} \tag{9}$$

where $[m]$ is the element mass matrices, $[k]$ is the linear stiffness matrices, and $[k1]$ and $[k2]$ are the first- and second-order nonlinear stiffness matrices.

E. System Equations

When the element matrices are assembled in standard finite element procedure and the kinematic boundary conditions are applied, the system equations of motion can be expressed as

$$\begin{bmatrix} [M_b] & 0 & 0 \\ 0 & [M_m] & 0 \\ 0 & 0 & 0 \end{bmatrix} \begin{Bmatrix} \ddot{W}_b \\ \ddot{W}_m \\ \ddot{W}_\phi \end{Bmatrix} + \left(\begin{bmatrix} [K_b] & [K_{bm}] & [K_{b\phi}] \\ [K_{mb}] & [K_m] & [K_{m\phi}] \\ [K_{\phi b}] & [K_{\phi m}] & [K_\phi] \end{bmatrix} \right.$$

$$- \begin{bmatrix} [K1_{N\phi}] & 0 & 0 \\ 0 & 0 & 0 \\ 0 & 0 & 0 \end{bmatrix} + \begin{bmatrix} [K1_{Nm}] + [K1_{NB}] & [K1_{bm}] & [K1_{b\phi}] \\ [K1_{mb}] & 0 & 0 \\ [K1_{\phi b}] & 0 & 0 \end{bmatrix}$$

$$\left. + \begin{bmatrix} [K2_b] & 0 & 0 \\ 0 & 0 & 0 \\ 0 & 0 & 0 \end{bmatrix} \right) \begin{Bmatrix} W_b \\ W_m \\ W_\phi \end{Bmatrix} = \begin{Bmatrix} 0 \\ 0 \\ P_\varphi \end{Bmatrix} \tag{10}$$

where $[M]$ is the system mass matrices, $[K]$ is the linear stiffness matrices, and $[K1]$ and $[K2]$ are the first- and second-order nonlinear stiffness matrices. $\{W_b\}$ and $\{W_m\}$ are the system structural displacements, and $\{W_\phi\}$ is the electric DOF. Because this is a free vibration, no applied mechanical force is at the right-hand side. $\{P_\phi\}$ is the electrical charge draw to the electrodes. Notice that for an isotropic beam or symmetric composite plate, the bending and in-plane coupling terms will be null.

F. Self-Sensing Actuator

For self-sensing actuators, the structural displacements $\{W_b\}$ and $\{W_m\}$ can be combined together as $\{W\} = \{W_b, W_m\}^T$. This yields the two equations from Eq. (10) for the actuation and sensing equations as

$$[M]\{\ddot{W}\} + ([K_{lin}] + [K_1] + [K_2])\{W\} = -([K_{w\varphi}] + [K1_{w\varphi}])\{W_\varphi\} \tag{11}$$

$$([K_{\phi w}] + [K1_{\phi w}])\{W\} = \{P_\phi\} - [K_\phi]\{W_\phi\} \tag{12}$$

where $[K_{w\phi}]$, $[K_{\phi w}]$, and $[K1_{w\phi}]$ can be expressed as

$$[K_{w\phi}] = \left[[K_{b\phi}]\right] = [K_{\phi w}]^T, \qquad [K1_{w\phi}] = \begin{bmatrix} [K1_{b\phi}] \\ 0 \end{bmatrix} = [K1_{\phi w}]^T \tag{13}$$

For an isotropic beam or symmetric composite plate, the $[K_{bm}]$, $[K_{mb}]$, and $[K1_{NB}]$ are equal to zero, where $[K_{lin}]$, $[K_1]$, and $[K_2]$ can be expressed as

$$[K_{lin}] = \begin{bmatrix} [K_b] & 0 \\ 0 & [K_m] \end{bmatrix}$$

$$[K_1] = - \begin{bmatrix} [K1_{N\phi}] & 0 \\ 0 & 0 \end{bmatrix} + \begin{bmatrix} [K1_{Nm}] & [K1_{bm}] \\ & 0 \end{bmatrix}$$

$$[K_2] = \begin{bmatrix} [K2_b] & 0 \\ 0 & 0 \end{bmatrix} \tag{14}$$

Because the difference of the electric charge $\{P_\varphi\}$ and the product term of $[K_\varphi]$ and $\{W_\varphi\}$ is a sensing signal proportional to the structure DOF, the $\{P_\varphi\}$ needs to be measured to obtain the difference. Here we assume that perfect measurement of $\{P_\varphi\}$ is achieved, and so the sensing signal is known exactly. Then the sensor equation becomes

$$\{q^s\} = -([K_{\varphi w}] + [K1_{\varphi w}])\{W\} \tag{15}$$

where q^s is the sensing signal.

Because the nonlinear free vibration action is out-of-plane or bending in nature, only the bending moments are piezoelectrically induced. Thus, we assume the piezoelectric in-plane resultant force $\{N_\varphi\}$ is zero. The matrices $[K_{m\varphi}]$, $[K_{N\varphi}]$, and $[K1_{b\varphi}]$ are null. Furthermore, for thin plates, the in-plane natural frequencies usually are two to three orders higher than the bending frequencies; neglecting the in-plane inertia term will not bring significant error. Therefore,

system equations (11) and (15) become[25]

$$[M_b]\{\ddot{W}_b\} + ([K_b] + [K2])\{W_b\} = -[K_{b\varphi}]\{W_\varphi\} \tag{16}$$

$$\{q^s\} = \begin{bmatrix} -[K_{\varphi b}] & 0 \end{bmatrix} \begin{Bmatrix} W_b \\ W_m \end{Bmatrix} \tag{17}$$

where $[K2]$ can be expressed as

$$[K2] = [K2_b] - [K1_{bm}][K_m]^{-1}[K1_{mb}] + [K2_{Nm}(\{W_m\}_2)] \tag{18}$$

$$\{W_m\}_2 = [K_m]^{-1}[K1_{mb}]\{W_b\} \tag{19}$$

G. Modal Equations

Because, for a set of modal equations, there is no need to assemble and update the nonlinear stiffness matrices at each time integration step, the number of modal equations is much smaller than the structure DOF equations.[25] Apply a modal transformation to Eqs. (16) and (17) by expressing

$$\{W_b\} = \sum_{r=1}^{n} q_r(t)\{\varphi_r\} = \Phi\{q\} \tag{20}$$

The linear frequencies and the corresponding natural modes are obtained from the linear vibration of the system

$$\omega_r^2[M_b]\{\varphi_r\} = [K_b]\{\varphi_r\} \tag{21}$$

Because the nonlinear element stiffness matrices can be expressed in the element displacements $\{w_b\}$ and $\{w_m\}$, in turn, they can be expressed by the linear modes $\{\varphi_r\}$. Thus, the actuating equations of motion in modal coordinates become

$$[\bar{M}_b]\{\ddot{q}\} + ([\bar{K}] + [\bar{K}_{qq}])\{q\} = -[\bar{K}_{b\varphi}]\{W_\varphi\} \tag{22}$$

and the sensing equation is

$$\{q^s\} = -[\bar{K}_{\varphi b}]\{q\} \tag{23}$$

Then, in the preceding equations, the modal mass and linear stiffness matrices are

$$([\bar{M}_b], [\bar{K}]) = [\Phi]^T([M_b], [K_b])[\Phi] \tag{24}$$

The second-order nonlinear modal stiffness matrix is

$$[\bar{K}_{qq}] = [\Phi]^T \sum_{r=1}^{n}\sum_{s=1}^{n} q_r q_s \left([K2_b]^{rs} + [K2_{Nm}]^{rs} - [K1_{bm}]^r[K_m]^{-1}[K1_{mb}]^s\right)[\Phi] \tag{25}$$

and the modal piezoelectric control matrix is

$$[\bar{K}_{b\varphi}] = [\Phi]^T[K_{b\varphi}] = [\bar{K}_{\varphi b}]^T \tag{26}$$

H. Modal Participation

Regarding the natural modes that should be included in the response analysis, they can be determined from the modal participation values[7]

$$Par_{r-th} = \frac{\max|q_r|}{\sum_{s=1}^{n}\max|q_s|} \tag{27}$$

III. Control Method

A. System State-Space Model

Based on the modal equations of motion (22), a standard state-space model for control design and simulation can be formed. $\boldsymbol{X}$ is the system state vector, which consists of the modal amplitudes and velocities

$$\boldsymbol{X} = \begin{Bmatrix} q \\ \dot{q} \end{Bmatrix} \tag{28}$$

$\boldsymbol{U}$ is the control input and $\boldsymbol{Y}$ is the sensor output

$$\boldsymbol{U} = \{W_\varphi\} \tag{29}$$

$$\boldsymbol{Y} = \{q^s\} \tag{30}$$

The state-space form for the modal equations of motion is then

$$\dot{\boldsymbol{X}} = \bar{\boldsymbol{A}}\boldsymbol{X} + \boldsymbol{B}\boldsymbol{U}, \qquad \boldsymbol{Y} = \boldsymbol{C}\boldsymbol{X} + \boldsymbol{D}\boldsymbol{U} \tag{31}$$

where the system matrices are

$$\bar{\boldsymbol{A}} = \begin{bmatrix} 0 & I \\ -[\bar{M}_b]^{-1}[\bar{K}] & 0 \end{bmatrix} + \begin{bmatrix} 0 & 0 \\ -[\bar{M}_b]^{-1}[\bar{K}_{qq}] & 0 \end{bmatrix}$$

$$\boldsymbol{B} = \begin{bmatrix} 0 \\ -[\bar{M}_b]^{-1}[\bar{K}_{b\varphi}] \end{bmatrix}, \qquad \boldsymbol{C} = \begin{bmatrix} -[\bar{K}_{\varphi b}] & 0 \end{bmatrix}, \qquad \boldsymbol{D} = 0 \tag{32}$$

where $\bar{\boldsymbol{A}}$ is a real system state matrix. In designing a controller for the system, we use its linearization form by applying a Taylor series approach. In fact, the linearized result $\boldsymbol{A}$ matrix is the first part of $\bar{\boldsymbol{A}}$

$$\boldsymbol{A} = \begin{bmatrix} 0 & I \\ -[\bar{M}_b]^{-1}[\bar{K}] & 0 \end{bmatrix} \tag{33}$$

B. LQR Control

Here, an LQR is used for our system. This method seeks a solution for the linear full state feedback problem defined as

$$\boldsymbol{U} = -\boldsymbol{K}\boldsymbol{X} \tag{34}$$

which minimizes a quadratic performance index $\boldsymbol{J}$ that is a function of system states and control effort

$$\boldsymbol{J} = \int_0^\infty [\boldsymbol{X}^T\boldsymbol{Q}\boldsymbol{X} + \boldsymbol{U}^T\boldsymbol{R}\boldsymbol{U}]\,\mathrm{d}\boldsymbol{t} \tag{35}$$

where $\boldsymbol{Q}$ is a symmetric positive semidefinite state weighting and $\boldsymbol{R}$ is a symmetric positive definite control effort weighting. When Eq. (35) is minimized, the controller gain is

$$\boldsymbol{K} = \boldsymbol{R}^{-1}\boldsymbol{B}^T\boldsymbol{P} \tag{36}$$

where $\boldsymbol{P}$ is a positive definite symmetric matrix determined from the solution of the algebraic Riccati equation

$$\boldsymbol{A}^T\boldsymbol{P} + \boldsymbol{P}\boldsymbol{A} - \boldsymbol{P}\boldsymbol{B}\boldsymbol{R}^{-1}\boldsymbol{B}^T\boldsymbol{P} + \boldsymbol{Q} = 0 \tag{37}$$

C. EKF

To apply the LQR control, we have to know all of the states of the system. In fact, it is difficult for the sensor to give the accurate information for every state. Thus, the state estimator needs to be used like the linear Kalman filter. Linearized system equations are used, and nonlinear effects are not considered during the process. State estimation performance for large-amplitude limit-cycle amplitudes may deteriorate as a result.[25] We solve this problem by using the EKF.[39] It replaces the nominal trajectory based on the linearized system by the estimated trajectory, then evaluates the Taylor series about the estimated trajectory. Thus, if the system is sufficiently observable, the estimated trajectory is sufficiently close to actual trajectory and makes the estimation valid.

The nonlinear state estimation is

$$\dot{\hat{\boldsymbol{X}}} = \bar{\boldsymbol{A}}(\hat{\boldsymbol{X}}, \boldsymbol{t})\hat{\boldsymbol{X}} + \boldsymbol{B}\boldsymbol{U} + \boldsymbol{K}_e(\boldsymbol{t})(\boldsymbol{Y} - \boldsymbol{C}\hat{\boldsymbol{X}}) \tag{38}$$

$$\hat{\boldsymbol{Y}} = \boldsymbol{C}\hat{\boldsymbol{X}} \tag{39}$$

The EKF contains the nonlinearity for the system dynamics, which is linearized according to the traditional Kalman filter, accounting for the better robustness of the EKF. The EKF uses linear approximation over a very small range of the state space. Then the Riccati equation is solved to get the EKF gains. In fact, in our system, the

linear approximation is for every step of the iteration for a nonlinear system. The resulting linearization's range is much smaller than the linearization of the traditional Kalman filter (which is the same as the linearization for LQR). Thus, the EKF can provide a better state estimation.

The linear approximation matrix is

$$\boldsymbol{F}(t) \approx \left.\frac{\partial \boldsymbol{f}(\boldsymbol{x},t)}{\partial \boldsymbol{x}}\right|_{x=\hat{x}(t)} = \left.\begin{bmatrix} \frac{\partial \boldsymbol{f}_1}{\partial \boldsymbol{x}_1} & \frac{\partial \boldsymbol{f}_1}{\partial \boldsymbol{x}_2} & \frac{\partial \boldsymbol{f}_1}{\partial \boldsymbol{x}_3} & \cdots & \frac{\partial \boldsymbol{f}_1}{\partial \boldsymbol{x}_n} \\ \frac{\partial \boldsymbol{f}_2}{\partial \boldsymbol{x}_1} & \frac{\partial \boldsymbol{f}_2}{\partial \boldsymbol{x}_2} & \frac{\partial \boldsymbol{f}_2}{\partial \boldsymbol{x}_3} & \cdots & \frac{\partial \boldsymbol{f}_2}{\partial \boldsymbol{x}_n} \\ \frac{\partial \boldsymbol{f}_3}{\partial \boldsymbol{x}_1} & \frac{\partial \boldsymbol{f}_3}{\partial \boldsymbol{x}_2} & \frac{\partial \boldsymbol{f}_3}{\partial \boldsymbol{x}_3} & \cdots & \frac{\partial \boldsymbol{f}_3}{\partial \boldsymbol{x}_n} \\ \vdots & \vdots & \vdots & \ddots & \vdots \\ \frac{\partial \boldsymbol{f}_n}{\partial \boldsymbol{x}_1} & \frac{\partial \boldsymbol{f}_n}{\partial \boldsymbol{x}_2} & \frac{\partial \boldsymbol{f}_n}{\partial \boldsymbol{x}_3} & \cdots & \frac{\partial \boldsymbol{f}_n}{\partial \boldsymbol{x}_n} \end{bmatrix}\right|_{x=\hat{x}(t)} \tag{40}$$

where

$$\boldsymbol{f}(\boldsymbol{x},\boldsymbol{t}) = \dot{\boldsymbol{X}} = \bar{\boldsymbol{A}}\boldsymbol{X} + \boldsymbol{B}\boldsymbol{U} \tag{41}$$

$$\{\boldsymbol{X}\} = [\boldsymbol{x}_1, \boldsymbol{x}_2, \boldsymbol{x}_3, \boldsymbol{x}_4, \boldsymbol{x}_5, \boldsymbol{x}_6, \boldsymbol{x}_7, \boldsymbol{x}_8]^T \tag{42}$$

and the Riccati equation for EKF is

$$\dot{\boldsymbol{P}}_e(\boldsymbol{t}) = \boldsymbol{F}(\boldsymbol{t})\boldsymbol{P}_e(\boldsymbol{t}) + \boldsymbol{P}_e(\boldsymbol{t})\boldsymbol{F}(\boldsymbol{t})^T - \boldsymbol{P}_e(\boldsymbol{t})\boldsymbol{C}^T\boldsymbol{R}_e^{-1}\boldsymbol{C}\boldsymbol{P}_e(\boldsymbol{t}) + \boldsymbol{Q}_e \tag{43}$$

The EKF gain is

$$\boldsymbol{K}_e(\boldsymbol{t}) = \boldsymbol{P}_e(\boldsymbol{t})\boldsymbol{C}^T\boldsymbol{R}_e^{-1} \tag{44}$$

The preceding equations indicate that the EKF gain is evaluated online.

D. System Identification

In this paper, the parameter identification[40,41] with a linear structure is proposed to identify the frequency of limit-cycle oscillation (LCO). A commonly used linear model is the autoregressive exogenous (ARX) model with

$$y(k) = \alpha_1 y(k-1) + \alpha_2 y(k-2) + \cdots + \alpha_p y(k-p) + \beta_0 u(k) + \beta_1 u(k-1) + \beta_2 u(k-2) + \cdots + \beta_p u(k-p) \tag{45}$$

The output y and input u can be selected from measured data. The coefficients α_i and β_i, called observer Markov parameters, with $i = 1, 2, \ldots, p$, must be identified during operation. The parameter p is the order for the linear structure. When the simplification and accuracy of the frequency identification is considered, the ARX model in this paper is represented by a second-order equation involving only one output, y:

$$y(k) = -\alpha_1 y(k-1) - \alpha_2 y(k-2) \tag{46}$$

System parameters or Markov parameters α_i and β_i can be found by using the recursive least-squares method. Equation (45) can be written in a vector form

$$y(k) = \bar{\boldsymbol{Y}}\boldsymbol{v}_p(k-1) \tag{47}$$

where

$$\bar{\boldsymbol{Y}} = \begin{bmatrix} \alpha_1 & \alpha_2 & \cdots & \alpha_p & \beta_0 & \beta_1 & \beta_2 & \cdots & \beta_p \end{bmatrix} \tag{48}$$

$$\boldsymbol{v}_p(k-1) = \begin{bmatrix} y(k-1) \\ \vdots \\ y(k-p) \\ u(k) \\ \vdots \\ u(k-p) \end{bmatrix} \tag{49}$$

For different values of k, Eq. (47) can be written as

$$y = \bar{\boldsymbol{Y}}\boldsymbol{V}_p$$

$$y = [y(k) \quad y(k+1) \quad \cdots \quad y(k+N-p-1)] \tag{50}$$

where

$$\boldsymbol{V}_p = [\boldsymbol{v}_p(k-1) \quad \boldsymbol{v}_p(k) \quad \cdots \quad \boldsymbol{v}_p(k+N-p-2)]$$

$$k = p+1, p+2, \ldots \tag{51}$$

The integer N is the number of samples processed in the system identification. The system parameters, at time $(k+N-p-2)+1$, can be identified using the least-squares method:

$$\bar{\boldsymbol{Y}} = y\boldsymbol{V}_p^T\left[\boldsymbol{V}_p\boldsymbol{V}_p^T\right]^+ \tag{52}$$

The plus represents the pseudoinverse of matrix. Then, for our system,

$$y = [y(2)y(3)\cdots y(k)] = [-\alpha_1 - \alpha_2]\begin{bmatrix} y(1) & y(2) & \cdots & y(k-1) \\ y(0) & y(3) & \cdots & y(k-2) \end{bmatrix} \tag{53}$$

If transferred to the z domain, the characteristic equation corresponding to Eq. (46) is

$$z^2 + \alpha_1 z + \alpha_2 = 0 \tag{54}$$

This characteristic equation can be used to identify the LCO frequency. The first step is to find the roots of the characteristic equation. Then free vibration natural frequency is calculated using the relationship between Z domain and S domain for the poles

$$z = e^{sT} \tag{55}$$

where T is the sampling time. One of the roots of the characteristic equation is the discrete system pole

$$z = z_0 + jz_1 \tag{56}$$

It can be represented by

$$z = \sqrt{z_0^2 + z_1^2}(z_0' + jz_1') = e^{s_1 T}e^{js_2 T} \tag{57}$$

with

$$\sqrt{z_0^2 + z_1^2} = e^{s_1 T} \tag{58}$$

$$z_0' + jz_1' = e^{js_2 T} \tag{59}$$

where

$$z_0' = \frac{z_0}{\sqrt{z_0^2 + z_1^2}} \tag{60}$$

$$z_1' = \frac{z_1}{\sqrt{z_0^2 + z_1^2}} \tag{61}$$

For the discrete pole location z, one can calculate s_1 and s_2, then find the system pole $s_1 + js_2$ in the S domain

$$s_1 = (1/T)\,\ell n\sqrt{z_0^2 + z_1^2}, \qquad s_2 = \tan^{-1}(z_1'/z_2') \tag{62}$$

The free vibration natural frequency is

$$\omega_n = \sqrt{s_1^2 + s_2^2} \tag{63}$$

and the LCO period in seconds becomes

$$\boldsymbol{T}_p = 2\pi/\omega_n \tag{64}$$

E. Control Method with System Identification

For the nonlinear system in our case, when using an EKF without an accurate initial estimation of states at the time when control begins, it is hard to provide a good estimation of the states, which will greatly affect the control results. Because the system is periodic, for a certain frequency, the states values for different time points within the period are distinct. Before the controller is implemented, several frequency-state value relationships can be obtained. During the control stage, the sensors yield information about the displacement, from which the nonlinear frequency of the free vibration can be calculated. Through interpolation, certain state values can then be derived from the relationship between the frequency and state values at a particular time point. Thus, even if the system changes its frequency suddenly for some reason, the frequency can still be detected, and a good estimation of initial states can be obtained for the EKF.

To obtain the frequency-state value relationship, two steps are needed. First, based on material properties of the beams and plates, the relationship between nonlinear frequency and vibration amplitude can be derived. Curves expressing such relationships are shown in Sec. V. From such identified relationships and frequencies, the amplitude of the system can be obtained. Second, if the amplitude is known, state values of a particular time point can be calculated by a numerical method, namely, the shooting method.[42]

IV. Self-Sensing Actuator Placement

Placement of sensors and actuators is another important factor in suppression of the large-amplitude vibration of the system. Optimal locations for the sensors and actuators make the control very effective. On the contrary, bad locations may degrade the control results and even produce spillover of the system. Here we use the NFCG, H_2, and norm of Kalman filter estimation gain (NKFEG) methods to choose the optimal location for the self-sensing actuators.

For the NFCG norm method,[33,34] the sum of the square of every element of the LQR gain can be calculated when an actuator is placed at each element of the object. The higher the value for the location, the more control authority the actuator has for the location. When each NFCG norm is calculated for each location, locations with a higher NFCG norm are chosen to be the optimal locations for the self-sensing actuators.

For the H_2 norm method,[28] the H_2 norm of the transfer function can be used to obtain the response characteristic at the location where the actuator is placed. A higher H_2 norm represents a higher controllability. Locations with higher H_2 norms are chosen to be the optimal locations for the self-sensing actuators.

V. Results

A. Material Properties

The system equations of motion of the beam and the composite plate are transferred into modal equations. The time-domain numerical method is employed to obtain the LCO. The fourth-order Runge–Kutta method is used (see Ref. 43). Material properties of the isotropic beam, composite plate, and PZT5A are shown in Table 1.

B. Adaptive Beam Vibration Control

1. Dimensions of Beam

To suppress the large-amplitude nonlinear free vibration, a clamped beam is first considered. The dimension of the aluminum beam is of $102.87 \times 5.715 \times 0.1372\ \text{cm}^3$ ($40.5 \times 2.25 \times 0.054\ \text{in.}^3$), and the finite element mesh has been chosen as 24×1 for the whole beam model.

2. Placement of Self-Sensing Actuators

Two methods are used to decide the optimal locations of the self-sensing piezoelectric actuators. The NFCG method is used to find the optimal locations for the actuators. The result is shown in Fig. 1a. One can apply the NKFEG method to find the optimal locations for the sensors by calculating the norm of Kalman filter estimation gain. The result is shown in Fig. 1b. Then one can place the self-sensing actuators at the optimal locations for both actuators and sensors

Table 1 Material properties of isotropic beam, composite plate, and PZT5A

	Materials		
Parameter	Aluminum	Graphite–epoxy	PZT5A
Young's modulus, psi (N/m^2)	$E = 8.85 \times 10^6$ (6.10×10^{10})	$E_1 = 22.50 \times 10^6$ (15.5×10^{10}) $E_2 = 1.17 \times 10^6$ (8.07×10^9)	$E_p = 9.00 \times 10^6$ (6.21×10^{10})
Shear modulus, psi (N/m^2)	$G = 3.38 \times 10^6$ (2.33×10^{10})	$G_{12} = 0.66 \times 10^6$ (4.55×10^9)	$G_p = 3.46 \times 10^6$ (2.39×10^{10})
Poisson's ratio	$\nu = 0.31$	$\nu_1 = 0.22$ $\nu_2 = 0.011$	$\nu = 0.30$
Density (lb $\cdot$ s^2/in.^{4}) (kg/m^3)	$\rho = 2.54 \times 10^{-4}$ (2702)	$\rho = 1.458 \times 10^{-4}$ (1550)	$\rho_p = 7.10 \times 10^{-4}$ (7582)
Thickness, in. (m)	$h = 0.054$ (1.37×10^{-3})	$h = 0.054$ (1.37×10^{-3})	$h = 0.009$ (2.3×10^{-4})
Charge constant, in./V (m/V)			$d_{31} = -7.51 \times 10^{-9}$ (-1.91×10^{-10})
Electrode space, in. (m)			$h_k = 0.009$ (2.3×10^{-4})
Maximum voltage, V			$V_{\max} = 820$

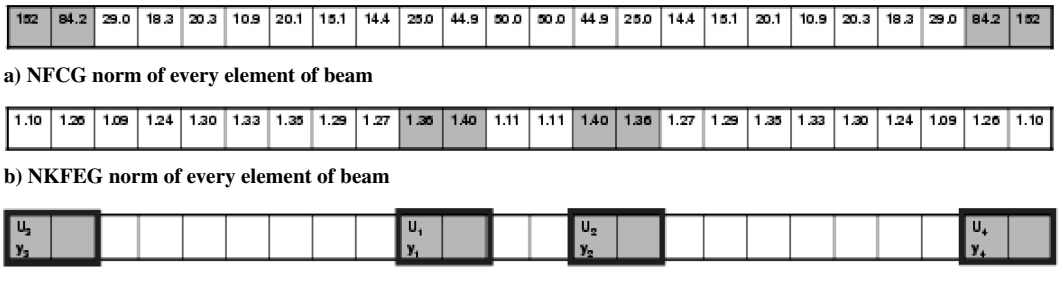

Fig. 1 Actuators' and sensors' locations on beam based on NFCG and NKFEG norms.

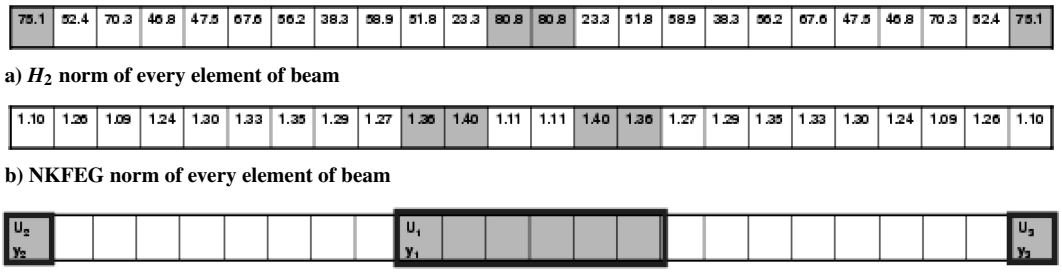

a) H_2 norm of every element of beam

b) NKFEG norm of every element of beam

c) Optimal locations based on two norms for beam

Fig. 2 Actuators' locations on beam based on H_2 and NKFEG norms.

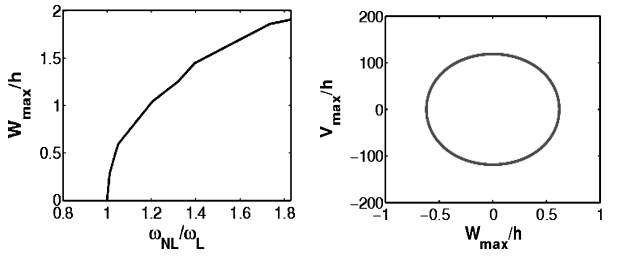

a) W_{max}/h vs frequency raio **c) Phase plot**

b) Time history **d) Power spectrum density**

Fig. 3 Free vibration response of clamped beam using four symmetric modes.

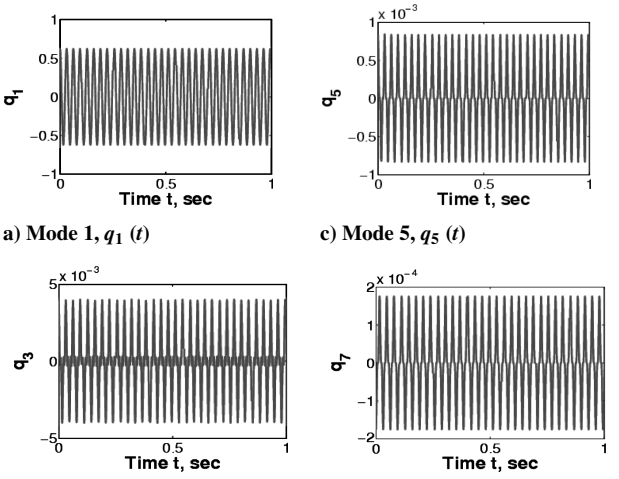

a) Mode 1, q_1 (t) **c) Mode 5, q_5 (t)**

b) Mode 3, q_3 (t) **d) Mode 7, q_7 (t)**

Fig. 4 Time histories of four symmetric modes for free vibration of clamped beam.

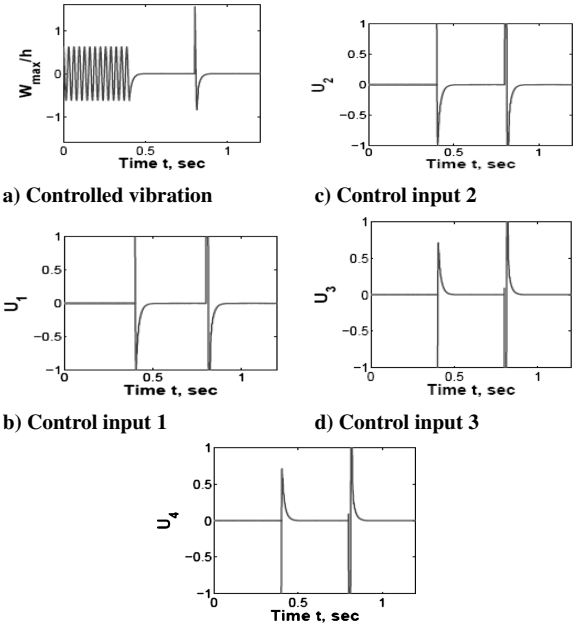

a) Controlled vibration **c) Control input 2**

b) Control input 1 **d) Control input 3**

e) Control input 4

Fig. 5 Displacement and control input for four-mode beam control using LQR/EKF under ideal estimation with NFCG and PZT5A.

as shown in Fig. 1c. Based on the optimal locations, four control inputs/outputs are used. The self-sensing actuators are bonded on the top and bottom surfaces of the beam using NFCG norm > 84 and NKFEG norm > 1.35.

One can repeat the whole process by using the H_2 norm method for optimal actuator locations. The result is shown in Fig. 2. Based on the optimal locations, three control inputs/outputs are used. Self-sensing actuators are placed at the locations where H_2 norm > 75 and NKFEG norm > 1.35.

3. Free Vibration of Beam

Results for free vibration of the beam with PZT5A and NFCG norms are shown in the following text. The relationship of the frequency ratio and W_{max}/h is shown in Fig. 3a. The time history, the phase plot, and the power spectrum density plot of the free vibration of the beam are shown in Figs. 3b–3d. The time histories of the first four symmetric modes, $q_1(t)$, $q_3(t)$, $q_5(t)$, and $q_7(t)$, are shown in Fig. 4. Obviously, it is an LCO.

4. Adaptive Beam Vibration Control with NFCG and PZT5A

The control of the beam vibration using LQR/EKF under ideal conditions is shown in Fig. 5. The control inputs shown in Table 1 are obtained through dividing the maximum control inputs shown. It is called ideal because in this case all of the initial states and unpredictable frequency changes of the system are known. Obviously, the EKF can easily give good state estimation, and LQR can control vibration very well. However, if the initial states of the system are unknown, EKF performance degrades dramatically and the controller fails to suppress the vibration in a short time. It is, thus, important to use system identification to provide accurate initial state estimation and modal frequency for the controller. This LQR/EKF with system identification is also called the adaptive LQR/EKF controller.

When the adaptive LQR/EKF controller is used, the relationship between system frequency ratio and the amplitude shown in Fig. 3a is used. Before the controller is implemented, five or six frequency ratios and corresponding amplitudes W_{max}/h are chosen. Then, corresponding to each known frequency ratio or amplitude W_{max}/h, all of the states at the initial or some other time can be obtained by the

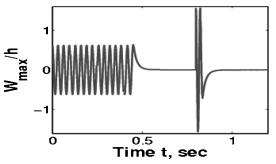

a) Controlled vibration

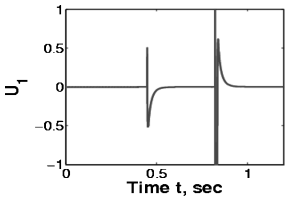

b) Control input 1

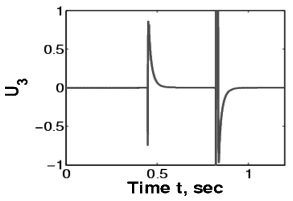

d) Control input 3

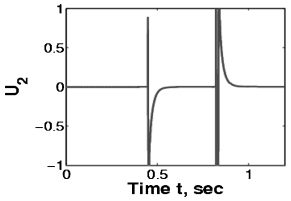

c) Control input 2

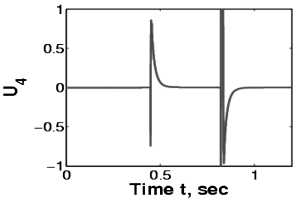

e) Control input 4

Fig. 6 Changed free vibration and adaptive control for four-mode beam clamped beam by using NFCG norm and PZT5A.

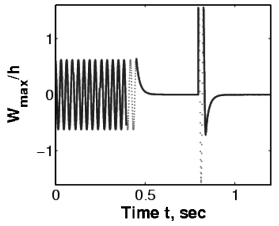

a) Controlled vibration with system identification

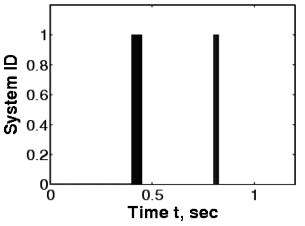

b) System identification working period

Fig. 7 System identification working period corresponding to controlled vibration.

shooting method. The relationship between frequency ratio and state values can, thus, be obtained. The system identification algorithm is implemented just before the controller is activated so that accurate estimated states can be used for the EKF. For the NFCG method case, the LQR/EKF is turned on at $t = 0.45$ and 0.826 s, so that the system identification is turned on during the periods from $t = 0.4$ to 0.45 s, and from $t = 0.8$ to 0.826 s. Figure 6 shows that the adaptive control efficiently suppress the vibration even when its amplitude changes suddenly at $t = 0.8$ s. Figure 7 shows the time period when the system identification is working.

From the sensors, the displacement information is known, and the nonlinear frequency ratio of the system can be calculated. Although multiple outputs exist, only the dominant one is used for frequency identification. Thus, only the output 1, which is obtained from the sensors at the maximum deflection, is used for both the NFCG and H_2 methods. For each frequency ratio, the state values can be obtained through interpolation. When the limit-cycle motion suddenly changes for some unpredictable cause, a new frequency ratio can be detected by the identification algorithm. After that, some state values for the vibration are determined. These values can be used as the updated initial state estimation for the EKF. Then, control for the system can be realized based on the updated initial state estimation. In the beam simulation, the system amplitude $W_{\max}/h$ changes suddenly from 0.6 to 1.2, and the adaptive control suppresses the vibration successfully.

5. Adaptive Beam Vibration Control with H_2 Norm and PZT5A

Another actuator placement method, the H_2 norm method, is considered. The results for adaptive control for these cases are shown in Fig. 8. From the control results, the overshooting and settling time of the condition of H_2 norm are almost the same as the NFCG method. When the control results are comparable, the actuators can be connected together as three pieces using H_2 norms instead of four pieces using NFCG (Figs. 1 and 2). When the number of inputs/outputs is larger, the connection of wires will be more complicated, and the corresponding method is more difficult to realize in practice. Thus, the H_2 norm method for optimal actuator locations is preferred here.

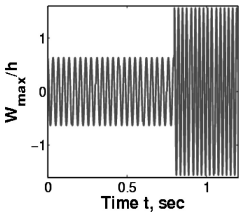

a) Free vibration

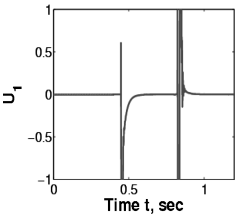

c) Control input 1

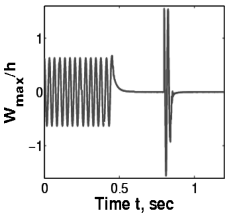

b) Controlled vibration

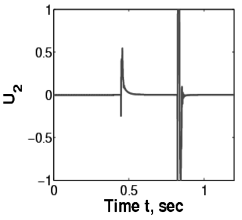

d) Control input 2

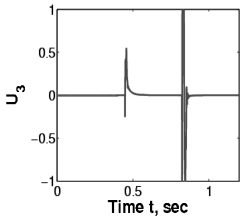

e) Control input 3

Fig. 8 Changed free vibration and adaptive control for clamped beam using H_2 norm.

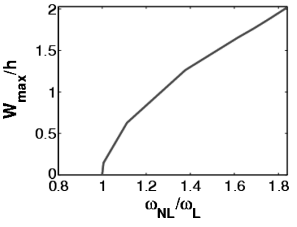

a) $W_{\max}/h$ vs frequency ratio

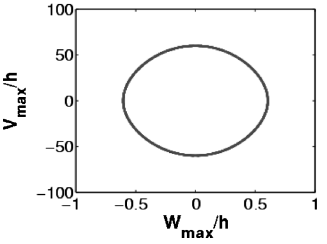

c) Phase plot

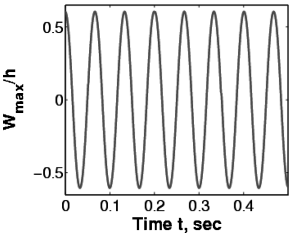

b) Time history

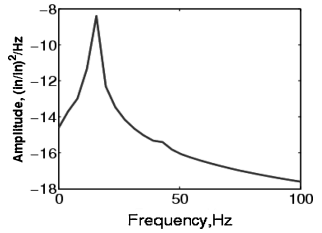

d) Power spectrum density

Fig. 9 Free vibration response of clamped composite plate using four lowest modes.

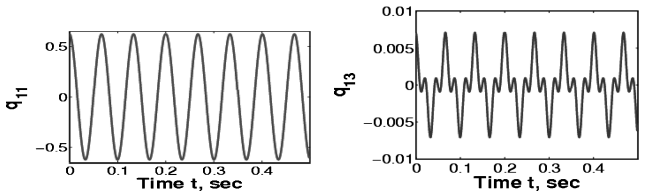

a) Mode (1, 1), q_{11} (t) c) Mode (1, 3), q_{13} (t)

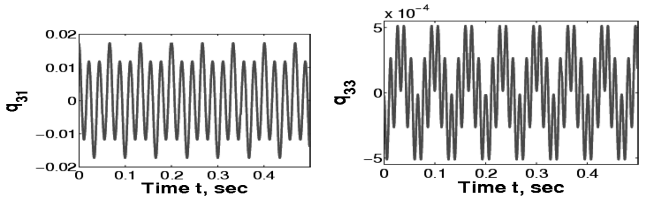

b) Mode (3, 1), q_{31} (t) d) Mode (3, 3), q_{33} (t)

Fig. 10 Time histories of four lowest modes for free vibration of clamped composite plate.

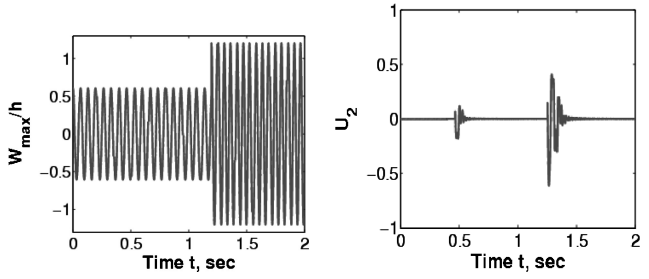

a) Free vibration d) Control input 2

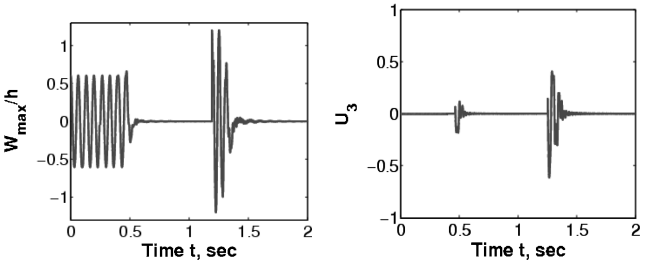

b) Controlled vibration e) Control input 3

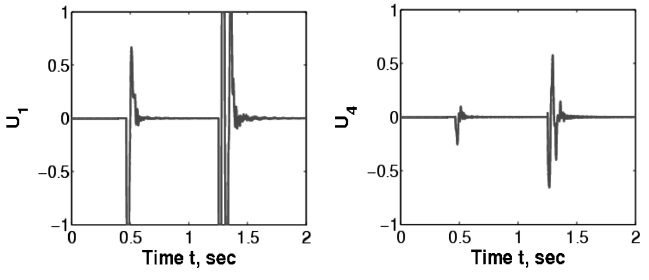

c) Control input 1 f) Control input 4

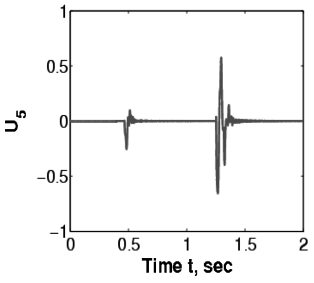

g) Control input 5

Fig. 11 Changed free vibration and adaptive control for four-mode clamped composite plate using NFCG and PZT5A.

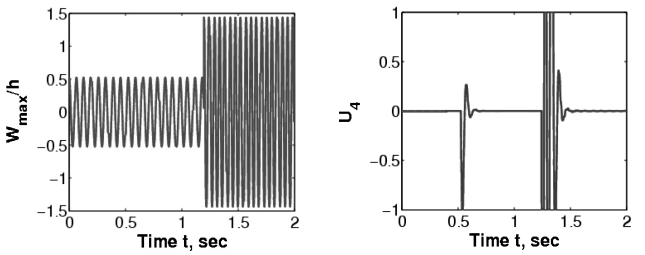

a) Free vibration f) Control input 4

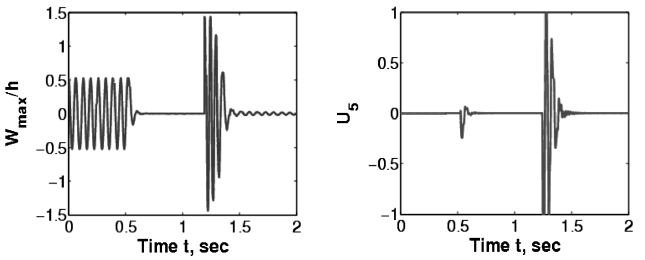

b) Controlled vibration g) Control input 5

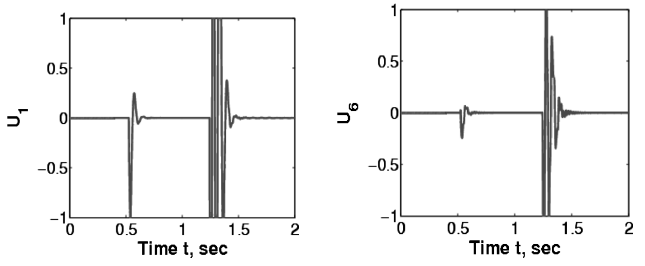

c) Control input 1 h) Control input 6

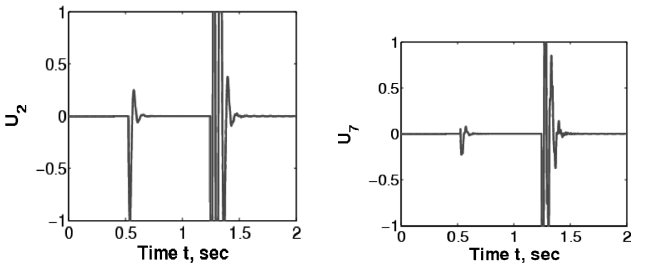

d) Control input 2 i) Control input 7

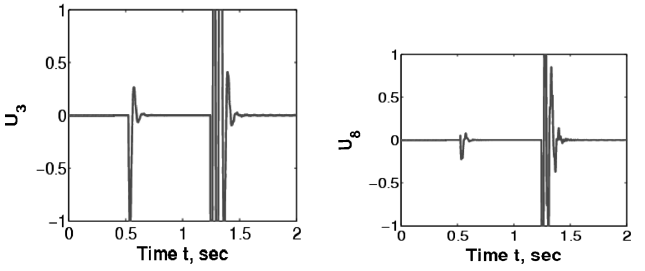

e) Control input 3 j) Control input 8

Fig. 12 Changed free vibration and adaptive control for four-mode clamped composite plate using H_2 norm and PZT5A.

C. Adaptive Composite Plate Vibration Control

The methods for the beam control and optimal location of self-sensing actuators can be applied to a clamped six-layer [0/60 deg/-60 deg]$_s$ rectangular composite plate. The composite plate is of $85.725 \times 57.15 \times 0.1372$ cm^3 ($33.75 \times 22.5 \times 0.054$ in.^{3}), and the mesh is 16×16 or 256 BFS elements for the full-plate model.

1. Placement of Self-Sensing Actuators

Based on the NFCG, H_2, and NKFEG norms, the locations of the self-sensing actuators for a whole plate are shown in Figs. A1 and A2 in the Appendix.

2. Free Vibration of Composite Plate

For the composite plate with PZT5A and NFCG norms, the results of the frequency ratio vs $W_{\max}/h$, time history of the free vibration, phase plot, and power spectrum density are shown in Fig. 9. It is clearly an LCO. Figure 10 shows the time history of the amplitudes of the four lowest symmetric modes: $q_{11}(t)$, $q_{31}(t)$, $q_{13}(t)$, and $q_{33}(t)$. The free vibration results are similar for the H_2 norm case.

3. Adaptive Composite Plate Vibration Control with NFCG, H_2, and PZT5A

The results for vibration control of the composite plate are shown in Figs. 11 and 12. The control performance of both the NFCG and H_2 norms is good. The optimal location of the self-sensing actuators based on the NFCG method shown in Fig. A1 is easier to implement because the number of inputs or outputs is five when using the NFCG but eight when using the H_2 norm shown in Fig. A2. The NFCG method for optimal actuator locations is preferred here for the sake of simplicity.

The LQR/EKF with system identification is a good method for the free vibration control. Especially when there is a sudden change in the amplitude/frequency, the system identification algorithm can supply accurate initial state values for the EKF in a very short time. With a good initial state estimation, the EKF can give a very good estimation to the LQR, and the LQR can supply an efficient control performance. Thus, the system identification works as a key part in the control because it decides the operation efficiency of the EKF and then decides the whole performance of the controller.

VI. Conclusions

The LQR with an EKF is used to suppress the nonlinear large-amplitude free vibrations. The results indicate that by linearizing the system in every time step, the EKF can provide a state estimation for the LQR control. However, if the free vibration is changed due to unpredictable causes, the LQR/EKF control approach results in poor performance in the suppression of the free vibration. In this study, a simple modal frequency identification algorithm is proposed. This algorithm can identify the changed modal frequency and update the accurate initial state estimation needed for EKF. From the beam and composite plate examples studied, the adaptive LQR/EKF controller is efficient in vibration suppression even in the presence of unpredictable sudden changes. For the optimal placement of the self-sensing actuators, the NFCG, H_2, and NKFEG norm methods are employed. For selecting optimal locations of self-sensing actuators, both the NFCG and H_2 norm methods are effective. Consideration is also given to the number of inputs/outputs used. The connection of self-sensing actuators is simpler for a smaller number of inputs/outputs.

This adaptive control of the free vibration of beams and composite plates is also a learning process for a more practical application on panel flutter suppression. As a self-excited, dynamic instability phenomenon, panel flutter is often encountered in supersonic and hypersonic flight vehicles, which can lead to the fatigue failure of skin panels. Suppression of panel flutter is important work in the aerospace field. The successful adaptive control of free vibration paves the way for future work in panel flutter suppression.

Appendix: Placement of Self-Sensing Actuators

1.48	6.74	19.6	30.9	36.4	22.9	34.5	44.8	45.6	33.5	10.3	5.91	5.52	2.91	1.52	1.03
2.73	1.5	1.36	1.74	2.87	3.92	4.3	4.6	4.79	5.3	3.37	2.14	1.39	1.24	1.4	1.22
7.97	1.4	10.1	20.5	19.8	21.5	34.3	34	20.5	10.7	10.7	20.7	20.7	4.03	1.23	2.04
17.5	2.28	19.4	39.5	33.9	26.3	51	61.5	44.2	20.4	17.3	50.4	51.9	24.7	1.26	4.36
32.1	4.89	22.6	42.3	33.8	14.3	32.4	64.3	48.3	17.9	7.28	32.9	56.4	34.7	1.55	9.21
38.4	3.39	20.5	45.2	39.2	8.9	19.4	64.8	57.5	20.9	2.31	13.9	16	9.68	2.35	18.6
41.8	3.45	23	45.5	49.7	12.1	21.4	61	74.8	31.5	5.51	19.6	24.8	14.7	4.14	34.4
40	3.69	22.9	45.5	47.7	19	32.1	65.1	71.6	39.6	16.1	34.3	33.3	17.3	4.36	35.8
35.8	4.36	17.3	33.3	34.3	16.1	39.6	71.6	65.1	32.1	19	47.7	45.5	22.9	3.69	40
34.4	4.14	14.7	24.8	19.6	5.51	31.5	74.8	61	21.4	12.1	49.7	45.5	23	3.45	41.8
18.6	2.35	9.68	16	13.9	2.31	20.9	57.5	64.8	19.4	8.9	39.2	46.2	20.5	3.39	38.4
9.21	1.55	34.7	56.4	32.9	7.28	17.3	48.3	64.3	32.4	14.3	33.8	42.3	22.6	4.89	32.1
4.36	1.26	24.7	51.9	50.4	17.3	20.4	44.2	61.5	51	26.3	33.9	39.5	19.4	2.28	17.5
2.04	1.23	4.03	20.7	20.7	10.7	10.7	20.5	34	34.3	21.5	19.8	20.5	10.1	1.4	7.97
1.22	1.4	1.24	1.39	2.14	3.37	5.3	4.79	4.6	4.3	3.92	2.87	1.74	1.36	1.5	2.73
1.03	1.52	2.91	5.52	5.91	10.3	33.5	45.6	44.8	34.5	22.9	36.4	30.9	19.6	6.74	1.48

a) NFCG of every element of composite plate

4	4	4	4	4	5.62	5.33	5.64	6.67	5.69	4.5	4	4.39	4	4	4
4	4.01	4	4	4.06	4.06	4.04	4.02	4.01	4.01	4.01	4	4.06	4.03	4	4
4	4	4	4	4	6.28	6.39	6	5.38	4.96	3.98	4	4	4	4.04	4
4	4	5.24	4	4	4	8.21	8.22	6.81	5.78	5.06	4	4.01	4	4	4
4	4.05	5.72	5.97	4	4	6.4	7.53	6.36	4.97	4.84	4	4.01	4.01	4	4
4.47	4.1	4.01	4	4	4.86	4.17	6.27	5.33	5.16	4.56	4.26	4	4.98	4.01	4
6.03	4.13	4.22	8.13	6.76	5.3	4.04	5.85	5.96	5.8	5.01	5.72	6.49	5.73	4.01	5.06
6.08	4.1	4.24	8.57	7.66	6.64	4.05	7.36	7.3	4.05	6.2	7.21	7.87	4.18	4.05	5.82
5.82	4.05	4.18	7.87	7.21	6.2	4.05	7.3	7.36	4.05	6.64	7.66	8.57	4.24	4.1	6.08
5.06	4.01	5.73	6.49	5.72	5.01	5.8	5.96	5.85	4.04	5.3	6.76	8.13	4.22	4.13	6.03
4	4.01	4.98	4	4.26	4.55	5.16	5.33	6.27	4.17	4.86	4	4	4.01	4.1	4.47
4	4	4.01	4.01	4	4.84	4.97	6.36	7.53	6.4	4	4	5.97	5.72	4.04	4
4	4	4	4.01	4.01	5.06	5.78	6.81	8.22	8.21	4	4	4	5.24	4	4
4	4.04	4	4	4	4.05	4.96	5.38	6	6.39	6.28	4	4	4	4	4
4	4	4.03	4.06	4	4.01	4.01	4.01	4.02	4.04	4.06	4.06	4	4	4.01	4
4	4	4	4.39	4	4.5	5.69	6.67	5.64	5.33	5.62	4	4	4	4	4

b) NKFEG of every element of composite plate

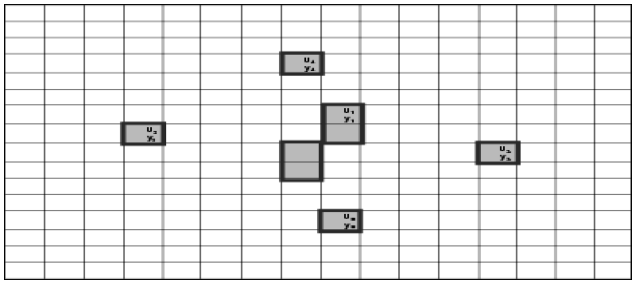

c) Optimal locations based on two norms for composite plate

Fig. A1 Optimal locations of self-sensing actuator on composite plate based on NFCG and NKFEG.

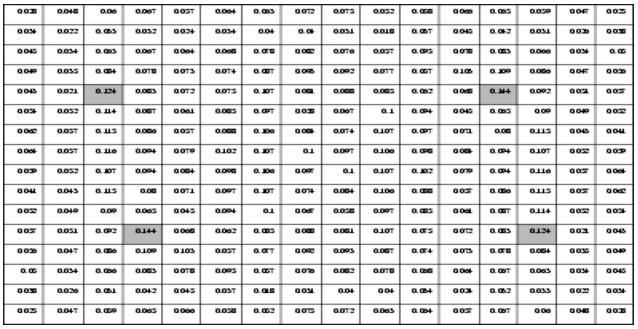

a) H_2 norm of every element of composite plate

4	4	4	4	4	5.62	5.33	5.64	6.67	5.69	4.5	4	4.39	4	4	4
4	4.01	4	4	4.06	4.06	4.04	4.02	4.01	4.01	4.01	4	4.06	4.03	4	4
4	4	4	4	4	6.28	6.39	6	5.38	4.96	3.98	4	4	4	4.04	4
4	4	5.24	4	4	4	8.21	8.22	6.81	5.78	5.06	4	4.01	4	4	4
4	4.05	5.72	5.97	4	4	6.4	7.53	6.36	4.97	4.84	4	4.01	4.01	4	4
4.47	4.1	4.01	4	4	4.86	4.17	6.27	5.33	5.16	4.56	4.26	4	4.98	4.01	4
6.03	4.13	4.22	8.13	6.76	5.3	4.04	5.85	5.96	5.8	5.01	5.72	6.49	5.73	4.01	5.06
6.08	4.1	4.24	8.57	7.66	6.64	4.05	7.36	7.3	4.05	6.2	7.21	7.87	4.18	4.05	5.82
5.82	4.05	4.18	7.87	7.21	6.2	4.05	7.3	7.36	4.05	6.64	7.66	8.57	4.24	4.1	6.08
5.06	4.01	5.73	6.49	5.72	5.01	5.8	5.96	5.85	4.04	5.3	6.76	8.13	4.22	4.13	6.03
4	4.01	4.98	4	4.26	4.55	5.16	5.33	6.27	4.17	4.86	4	4	4.01	4.1	4.47
4	4	4.01	4.01	4	4.84	4.97	6.36	7.53	6.4	4	4	5.97	5.72	4.04	4
4	4	4	4.01	4.01	5.06	5.78	6.81	8.22	8.21	4	4	4	5.24	4	4
4	4.04	4	4	4	4.05	4.96	5.38	6	6.39	6.28	4	4	4	4	4
4	4	4.03	4.06	4	4.01	4.01	4.01	4.02	4.04	4.06	4.06	4	4	4.01	4
4	4	4	4.39	4	4.5	5.69	6.67	5.64	5.33	5.62	4	4	4	4	4

b) NKFEG of every element of composite plate

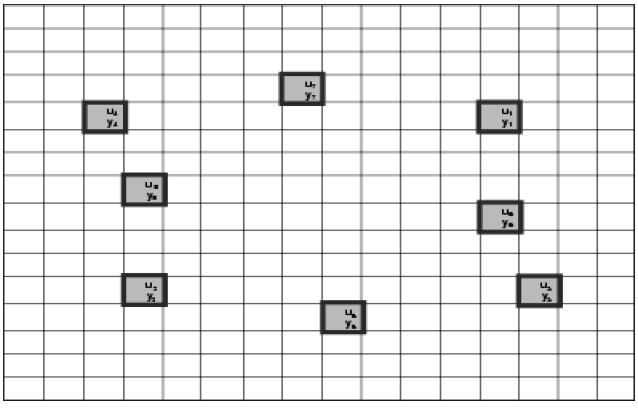

c) Optimal locations based on two norms for composite plate

Fig. A2 Optimal locations of self-sensing actuator on composite plate based on H_2 norm and NKFEG.

References

[1]Woinowsky-Krieger, S., "The Effect of an Axial Force on the Vibration of Hinged Bars," *Journal of Applied Mechanics*, Vol. 17, No. 1, 1950, pp. 35–36.

[2]Chu, H. N., and Herrmann, G., "Influence of Large Amplitudes on Free Flexural Vibrations of Rectangular Elastic Plates," *Journal of Applied Mechanics*, Vol. 23, No. 4, 1956, pp. 532–540.

[3]Srinivasan, A. V., "Nonlinear Vibrations of Beams and Plates," *International Journal of Nonlinear Mechanics*, Vol. 1, No. 3, 1966, pp. 179–191.

[4]Ray, J. D., and Bert, C. W., "Nonlinear Vibrations of a Beam with Pinned Ends," *Journal of Engineering for Industry*, Vol. 91, No. 4, 1969, pp. 997–1004.

[5]Mei, C., "Nonlinear Vibration of Beams by Matrix Displacement Method," *AIAA Journal*, Vol. 10, No. 3, 1972, pp. 355–357.

[6]Srirangarajan, H. R., "Nonlinear Free Vibrations of Uniform Beams," *Journal of Sound and Vibration*, Vol. 175, No. 3, 1994, pp. 425–427.

[7]Shi, Y., Lee, R. Y. Y., and Mei, C., "Finite Element Method for Nonlinear Free Vibrations of Composite Plates," *AIAA Journal*, Vol. 35, No. 1, 1997, pp. 159–166.

[8]Saha, K. N., Misra, D., Pohit, G., and Ghosal, S., "Large Amplitude Free Vibration Study of Square Plates Under Different Boundary Conditions Through a Static Analysis," *Journal of Vibration and Control*, Vol. 10, No. 7, 2004, pp. 1009–1028.

[9]Rao, S. R., Sheikn, A. H., and Mukhopadhyay, M., "Large-Amplitude Finite Element Flexural Vibration of Plates/Stiffened Plates," *Journal of the Acoustical Society of America*, Vol. 93, No. 6, 1993, pp. 3250–3257.

[10]Mei, C., "Finite Element Displacement Method for Large Amplitude Free Flexural Vibrations of Beams and Plates," *Computers and Structures*, Vol. 3, No. 1, 1973, pp. 163–174.

[11]Chia, C. Y., "Geometrically Nonlinear Behavior of Composite Plates: A Review," *Applied Mechanics Reviews*, Vol. 41, No. 12, 1988, pp. 439–451.

[12]Alhazza, K. A., and Alhazza, A. A., "A Review of the Vibrations of Plates and Shells," *Shock and Vibration Digest*, Vol. 36, No. 5, 2004, pp. 377–395.

[13]Harada, A., Kobayashi, Y., and Yamada, G., "Reduced-Order Nonlinear Modal Equations of Plates Based on the Finite Element Method," *Eighth International Conference on Recent Advances in Structural Dynamics*, Southampton, England, U.K., 2003.

[14]Mei, C., Mace, B. R., and Jones, R. W., "Hybrid Wave/Mode Active Vibration Control," *Journal of Sound and Vibration*, Vol. 247, No. 5, 2001, pp. 765–784.

[15]Halkyard, C. R., and Mace, B. R., "Feedforward Adaptive Control of Flexural Vibration in a Beam Using Wave Amplitude," *Journal of Sound and Vibration*, Vol. 254, No. 1, 2002, pp. 117–141.

[16]Inman, D. J., "Active Modal Control for Smart Structures," *Philosophical Transactions: Mathematics, Physical and Engineering Sciences*, Vol. 359, No. 1778, 2001, pp. 205–219.

[17]Meirovitch, L., Baruh, H., and Oz, H., "A Comparison of Control Techniques for Large Flexible Systems," *Journal of Guidance, Control, and Dynamics*, Vol. 6, No. 4, 1983, pp. 302–310.

[18]Xie, S. L., Zhang, X. N., Zhang, J. H., and Yu, L., "H1 Robust Vibration Control of a Thin Plate Covered with a Controllable Constrained Damping Layer," *Journal of Vibration and Control*, Vol. 10, No. 1, 2004, pp. 115–133.

[19]Yu, Y. G., and Zhang, S. C., "Adaptive Backstepping Sychronization of Uncertain Chaotic System," *Chaos, Solitons and Fractals*, Vol. 21, No. 3, 2004, pp. 643–649.

[20]Hossain, M. A., Madkour, A. A. M., Dahal, K. P., and Yu, H., "Intelligent Active Vibration Control for a Flexible Beam System," *Proceedings of the IEEE SMC UK-RI Chapter Conference 2004 on Intelligent Cybernetic Systems*, Inst. of Electrical and Electronics Engineers, Londonderry, England, U.K., 2004, pp. 85–89.

[21]Narayanan, S., and Balamurugan, V., "Finite Element Modelling of Piezolaminated Smart Structures for Active Vibration Control with Distributed Sensors and Actuators," *Journal of Sound and Vibration*, Vol. 262, No. 3, 2003, pp. 529–562.

[22]Moita, J. M. S., Correia, I. F. P., Soares, C. M. M., and Soares, C. A. M., "Active Control of Adaptive Laminated Structures with Bonded Piezoelectric Sensors and Actuators," *Computers and Structures*, Vol. 82, No. 17, 2004, pp. 1349–1358.

[23]Williams, R. B., and Inman, D. J., "An Overview of Composite Actuators with Piezoceramic Fibers," *Proceedings of the 20th International Modal Analysis Conference*, Los Angeles, 2002.

[24]Schultz, M. R., and Hyer, M. W., "A Morphing Concept Based on Unsymmetric Composite Lamminate and Piezoceramic MFC Actuators," *45th AIAA/ASME/ASCE/AHS/ASC Structures, Structural Dynamics, and Materials Conference*, Vol. 1806, AIAA, Reston, VA, 2004, pp. 1–13.

[25]Abdel-Motagaly, K., "Finite Element Analysis and Active Control for Nonlinear Flutter of Composite Panes Under Yawed Supersonic Flow," Ph.D. Dissertation, Dept. of Aerospace Engineering, Old Dominion Univ., Norfolk, VA, Dec. 2001.

[26]Gawronski, W. K., "Actuator and Sensor Placement for Structural Testing and Control," *Journal of Sound and Vibration*, Vol. 208, No. 1, 1997, pp. 101–109.

[27]Wang, S. Y., Quek, S. T., and Ang, K. K., "Optimal Placement of Piezoelectric Sensor/Actuator Pairs for Vibration Control of Composite Plates," *Smart Structures and Materials 2002: Modeling, Signal Processing, and Control*, edited by V. S. Rao, Vol. 4693, Society of Photo-Optical and Instrumentation Engineers, San Diego, CA, 2002, pp. 461–471.

[28]Halim, D., and Moheimani, S. O. R., "An Optimization Approach to Optimal Placement of Collocated Piezoelectric Actuators and Sensors on a Thin Plate," *Mechatronics*, Vol. 13, No. 1, 2003, pp. 27–47.

[29]Demetriou, M. A., and Grigoriadis, K. M., "Collocated Actuator Placement in Structural Systems Using an Analytical Bound Approach," *Proceedings of the 2004 American Control Conference*, Boston, 2004, pp. 1604–1608.

[30]Demetriou, M. A., "A Numerical Algorithm for the Optimal Placement of Actuators and Sensors for Flexible Structures," *Proceedings of the 2004 American Control Conference*, Chicago, 2000, pp. 2290–2294.

[31]Beven, J. S., "Piezoceramic Actuator Placement for Acoustic Control of Panels," NASA CR-2001-211265, Dec. 2001.

[32]Maxwell, N. D., and Asokanthan, S. F., "Optimally Distributed Actuator Placement and Control for a Slewing Single-Link Flexible Manipulator," *Smart Materials and Structures*, Vol. 12, No. 2, 2003, pp. 287–296.

[33]Zhou, R. C., Lai, Z. H., Xue, D. Y., Huang, J. K., and Mei, C., "Suppression of Nonlinear Panel Flutter with Piezoelectric Actuators Using Finite Element Method," *AIAA Journal*, Vol. 33, No. 6, 1995, pp. 1098–1105.

[34]Zhou, R. C., Mei, C., and Huang, J.-K., "Suppression of Nonlinear Panel Flutter at Supersonic Speeds and Elevated Temperatures," *AIAA Journal*, Vol. 34, No. 2, 1996, pp. 347–354.

[35]Bogner, F. K., Fox, R. L., and Schmit, L. A., "The Generation of Inter-Element Compatible Stiffness and Mass Matrices by the Use of Interpolation Formulas," U.S. Air Force Flight Dynamics Lab., Technical Rept. AFFDL-TR-66-80, Wright–Patterson AFB, OH, Nov. 1966, pp. 397–444.

[36]Jones, R. M., *Mechanics of Composite Materials*, 2nd ed., Taylor & Francis, Philadephia, 1999, pp. 55–119.

[37]Bevan, J. S., "Analysis and Testing of Plates with Piezoelectric Sensors and Actuators," M.S. Thesis, Dept. of Aerospace Engineering, Old Dominion Univ., Norfolk, VA, May 1997.

[38]Guo, X., "Shape Memory Alloy Applications on Control of Thermal Buckling, Panel Flutter and Random Vibration of Composite Panels," Ph.D. Dissertation, Dept. of Aerospace Engineering, Old Dominion Univ., Norfolk, VA, May 2005.

[39]Grewal, M. S., and Andrews, A. P., *Kalman Filtering: Theory and Practice Using MATLAB*, 2nd ed., Wiley, New York, 2001, pp. 175–184.

[40]Chen, C.-W., Juang, J.-N., and Huang, J.-K., "Adaptive Linear System Identification and State Estimation," *Control and Dynamic Systems: Advances in Theory and Applications*, Vol. 57, Multidisciplinary Engineering Systems: Design and Optimization Techniques and Their Application, edited by C. T. Leondes, Academic Press, San Diego, CA, 1993, pp. 331–368.

[41]Hsiao, M.-H., Huang, J.-K., and Cox, D. E., "Iterative LQG Controller Design Through Closed-Loop Identification," *Journal of Dynamic Systems, Measurement and Control*, Vol. 118, No. 2, 1996, pp. 366–372.

[42]Przekop, A., "Nonlinear Response and Fatigue Estimation of Aerospace Curved Surface Panels to Acoustic and Thermal Loads," Ph.D. Dissertation, Dept. of Aerospace Engineering, Old Dominion Univ., Norfolk, VA, Dec. 2003.

[43]Dormand, J. R., and Prince, P. J., "A Family of Embedded Runge–Kutta Formulae," *Journal of Computational and Applied Mathematics*, Vol. 6, No. 1, 1980, pp. 19–26.

A. Palazotto
Associate Editor